JOURNAL OF SPACECRAFT AND ROCKETS
Vol. 30, No. 3, May–June 1993

Extension of Unsteady Embedded Newtonian Theory

L. E. Ericsson* and H. H. C. King†
Lockheed Missiles & Space Company, Inc., Sunnyvale, California 94086

A previously developed unsteady embedded Newtonian theory has been extended to be able to predict the hypersonic unsteady aerodynamics of axisymmetric bodies of general shape with the accuracy needed for preliminary design. The static aerodynamics determined by a three-dimensional finite difference method are used together with unsteady embedded Newtonian flow concepts to provide the vehicle dynamics without significantly adding computational time to the static computer program.

Nomenclature

C_γ, C_0 = proportionality constants [see Appendix, Eqs. (A2) and (A9), respectively]
c = reference length, d_B for conical bodies
D_N = nose drag, coefficient $C_{DN}=D_N/(\rho_\infty U_\infty^2/2)(\pi d_N^2/4)$
d_B, d_N = base diameter, nose (bluntness) diameter
f = pressure correlation function
f^* = dynamic pressure ratio, $\rho U^2/\rho_\infty U_\infty^2$
f_{bo} = lower bound of f^*
g^* = velocity ratio, U/U_∞
L = cylinder-flare body length
ℓ = sharp-cone body length
M = Mach number
M_p = pitching moment, coefficient $C_m=M_p/(\rho_\infty U_\infty^2/2)Sc$
N = normal force, coefficient $C_N=N/(\rho_\infty U_\infty^2/2)S$
p = static pressure, coefficient $C_p=(p-p_\infty)/(\rho_\infty U_\infty^2/2)$
p_0 = blast wave pressure, coefficient $C_{p0}=(p_0-p_\infty)/(\rho_\infty U_\infty^2/2)$
q = rigid-body pitch rate
R = radial distance from bow shock centerline, see Fig. 1
R_{sh} = bow shock radius, see Fig. 1
Re = Reynolds number, $Re_{\ell_\infty}=\ell U_\infty/\nu_\infty$
r = body radius, see Fig. 1
S = reference area, $\pi c^2/4$
t = time
U = axial velocity
x = axial coordinate, see Fig. 1
z = translatory coordinate, see Fig. 1
α = angle of attack
α_0 = trim angle of attack
γ = ratio of specific heats, =1.4 for air
Δ = difference or increment
ΔA = surface area element, see Fig. 1
$\Delta\bar{x}$ = cone center-of-gravity location forward of base
θ = body perturbation in pitch
θ_c = cone half-angle
θ_F = flare angle, see Fig. 1
ν = kinematic viscosity of air
ρ = air density
ϕ = azimuthal angle, see Fig. 1
χ = hypersonic similarity parameter defined in Eq. (A15)

Subscripts

B = base
CG = center of gravity or oscillation center
c = cone
F = flare
L = local
N = nose
Newt = Newtonian value
sh = bow shock
1, 2 = numbering subscripts used in the Appendix
∞ = freestream conditions

Superscript

i = induced, e.g., $\Delta^i C_p$ = nose-bluntness-induced pressure change on aft body

Derivative Symbols

$\dot{\theta}$ = $\partial\theta/\partial t$
C_{mq} = $\partial C_m/\partial(cq/U_\infty)$
$C_{m\dot{\alpha}}$ = $\partial C_m/\partial(c\dot{\alpha}/U_\infty)$
$C_{m\theta}$ = $\partial C_m/\partial\theta$
$C_{m\dot{\theta}}$ = $C_{mq}+C_{m\dot{\alpha}}$

Introduction

AT hypersonic speeds a blunt nose is often needed for thermodynamic survival. The nose-bluntness-induced curved bow shock generates a highly nonuniform flowfield, the "entropy wake," in which the aft body is embedded. Using the embedded Newtonian flow concept, the nonlinear unsteady aerodynamics of blunted cylinder-flare and conical body geometries could be predicted with the accuracy needed for preliminary design.[1] In the present paper the theory of Ref. 1 is extended to more general geometries by combining it with an existing theory for prediction of the static hypersonic aerodynamics of blunted bodies of general shape.[2]

Discussion

At high supersonic and hypersonic speeds a blunt nose generates a curved bow shock that in turn produces a nonuniform flow region, an entropy wake, in which the aft body is embedded[1] (Fig. 1). Figure 2 shows how the blast-wave pressure C_{p0}, the velocity ratio $g^*=U/U_\infty$, and the dynamic pressure ratio $f^*=\rho U^2/\rho_\infty U_\infty^2$ vary in the entropy wake region between the cylindrical aft body and the bow shock for a hemispherical nose.[3] For a cylinder-flare body the results shown in Fig. 3 are obtained.[1] For the chosen geometry the contribution by the flare to the static stability is roughly the same as in the case of a pointed, slender nose, for which the Newtonian theory gives a correct estimate. For the actual case of the hemisphere nose, this Newtonian effect ($C_{m\alpha L}$) is reduced greatly because of the reduction of the mean dynamic pressure in the entropy wake. However, the translation of the flare with increasing α through the inviscid shear flow to higher velocities and associated higher dynamic pressures, produces a statically

Received Jan. 18, 1992; revision received Nov. 27, 1992; accepted for publication Nov. 27, 1992.

*Retired; currently Engineering Consultant. Fellow AIAA.
†Currently with ETAK, Inc., Menlo Park, CA.

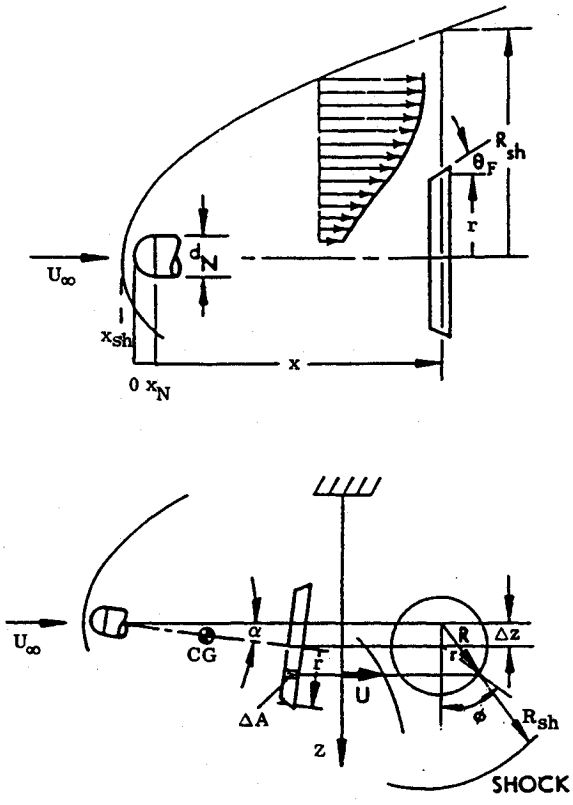

Fig. 1 Bow-shock-induced inviscid shear flow.

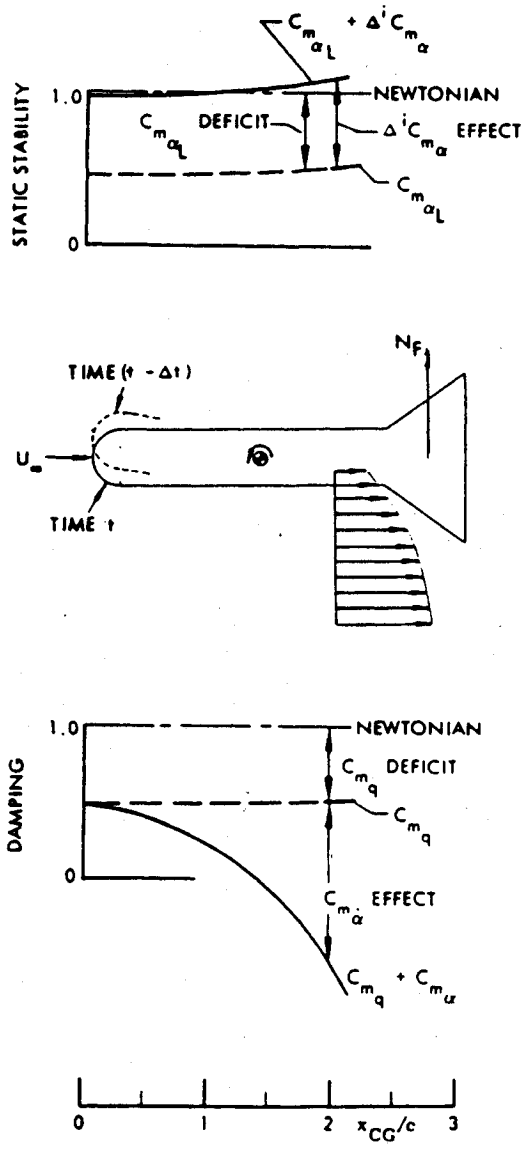

Fig. 3 Flare contribution to hypersonic static and dynamic stability at $\alpha=0$.[1]

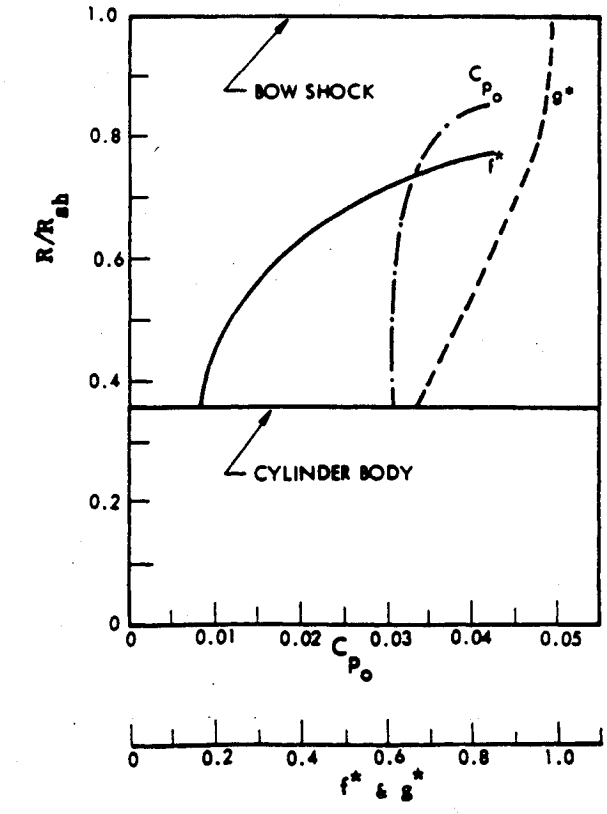

Fig. 2 Shear flow profiles 2.7 calibers aft of the bow shock of a hemisphere-cylinder at 20,000 fps.[1]

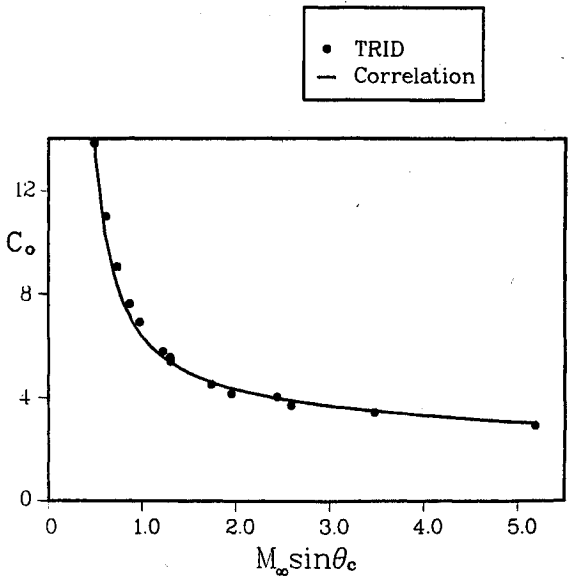

Fig. 4 Blast-wave correlation factor.

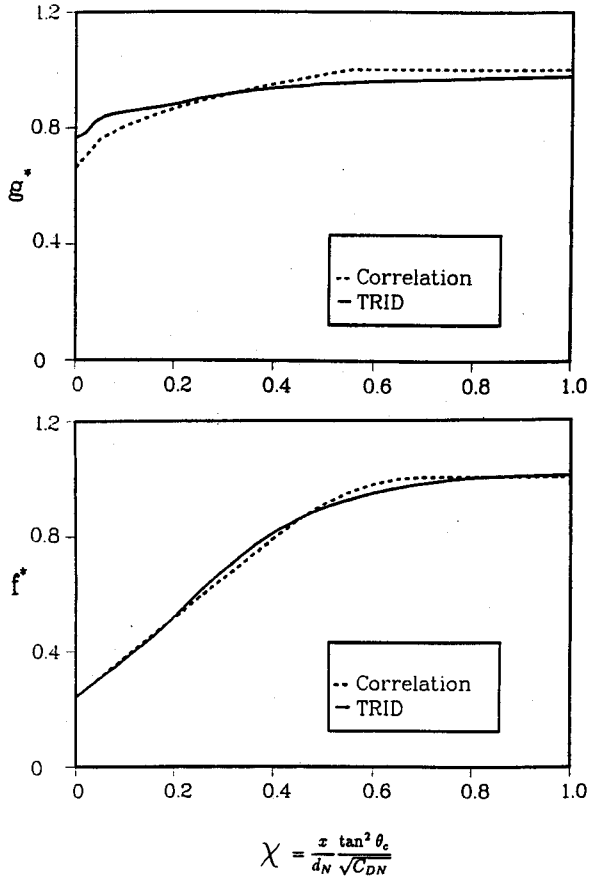

Fig. 5 Correlation functions for hypersonic shear flow parameters f^* and g^*.

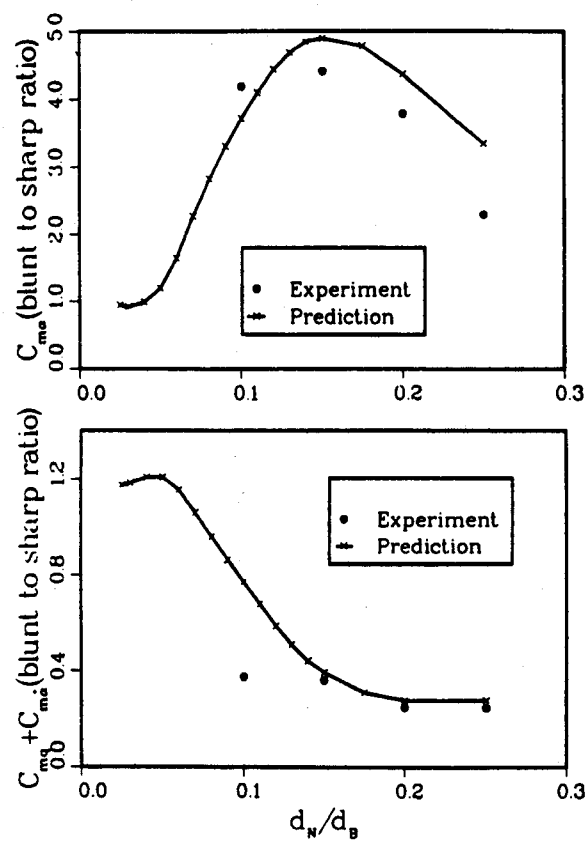

Fig. 6b Comparison between predicted and measured effect of nose bluntness on the static and dynamic derivatives of slender cones at M_∞=14, α=0, and θ_c=7 deg.

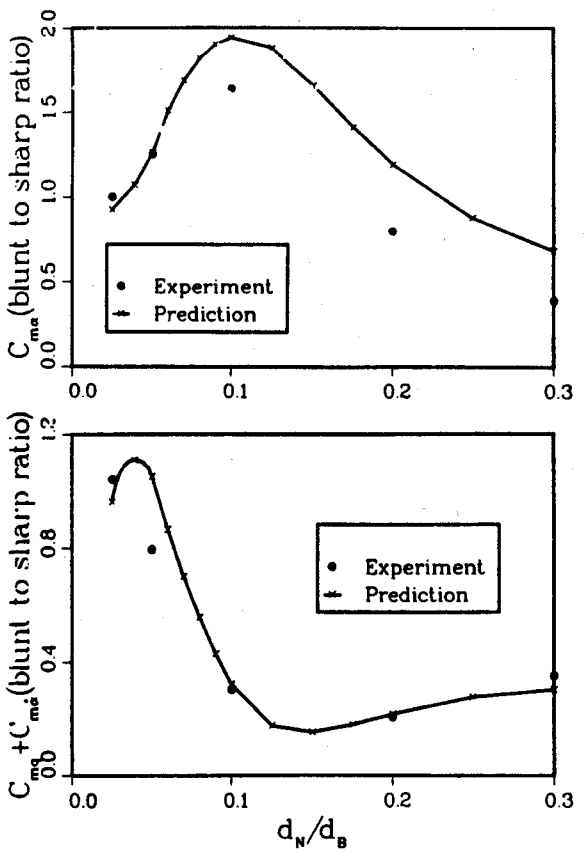

Fig. 6a Comparison between predicted and measured effect of nose bluntness on the static and dynamic derivatives of slender cones at M_∞=14, α=0, and θ_c=5.6 deg.

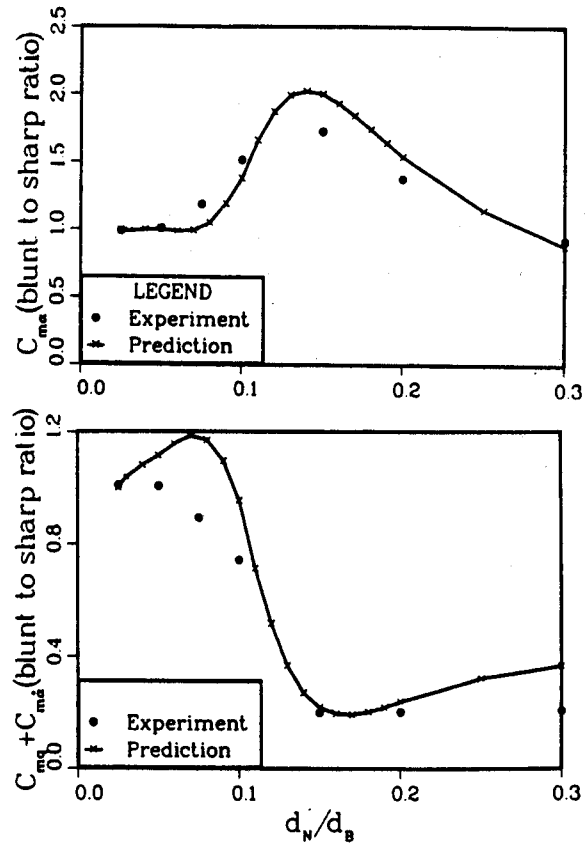

Fig. 6c Comparison between predicted and measured effect of nose bluntness on the static and dynamic derivatives of slender cones at M_∞=14, α=0, and θ_c=10 deg.

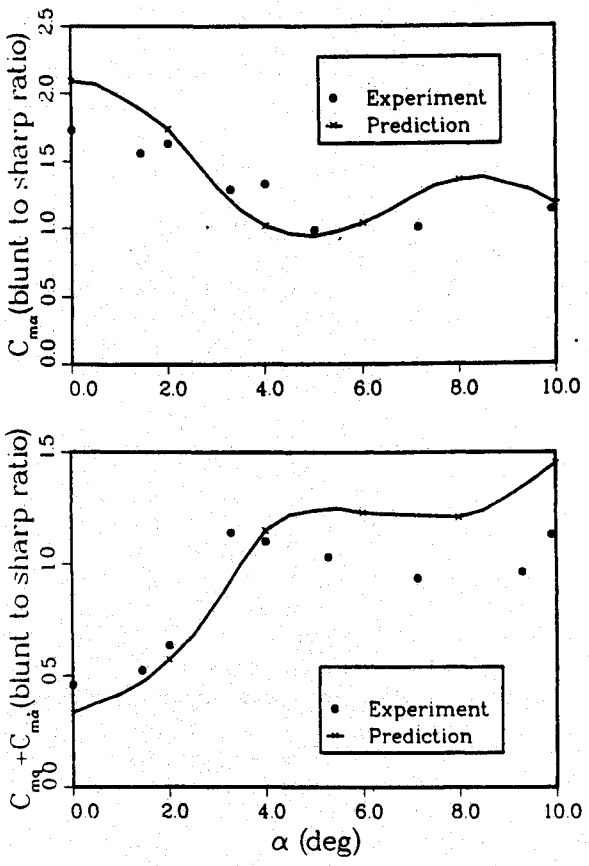

Fig. 7a Comparison between predicted and measured nose bluntness effects on a 5.6-deg cone at various angles of attack; d_N/d_B=0.1.

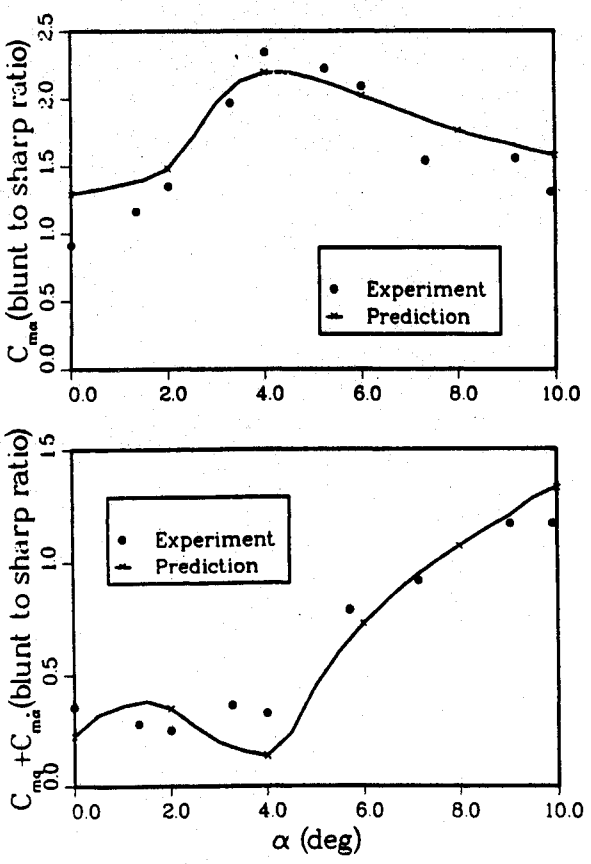

Fig. 7b Comparison between predicted and measured nose bluntness effects on a 5.6-deg cone at various angles of attack; d_N/d_B=0.2.

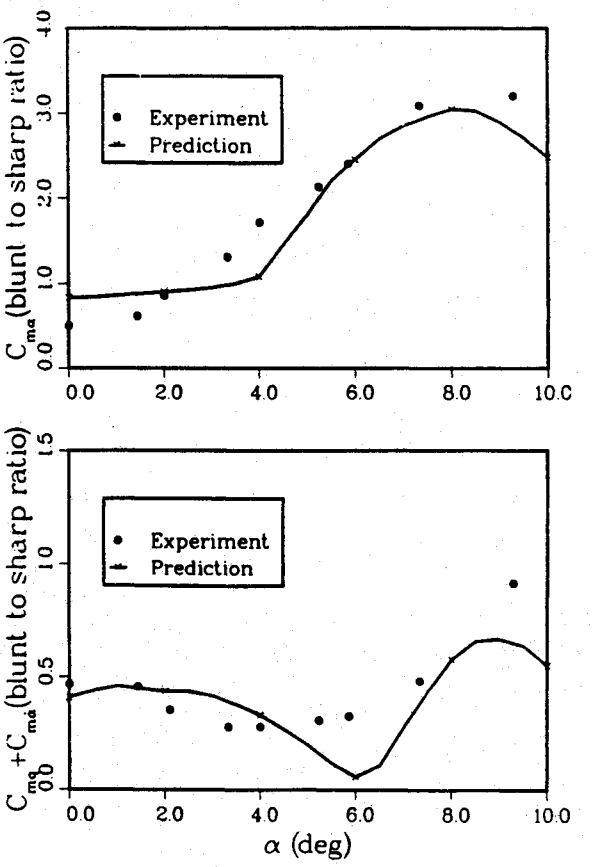

Fig. 7c Comparison between predicted and measured nose bluntness effects on a 5.6-deg cone at various angles of attack; d_N/d_B=0.3.

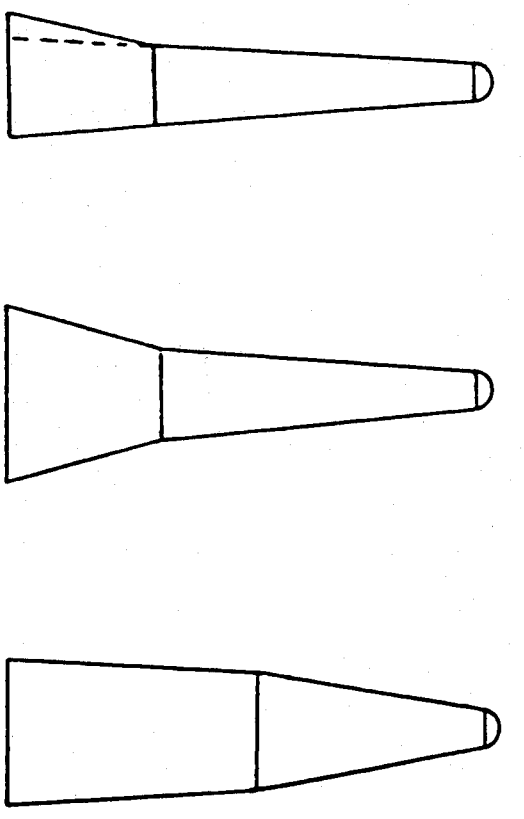

Fig. 8 Hypersonic vehicle geometries of future interest.

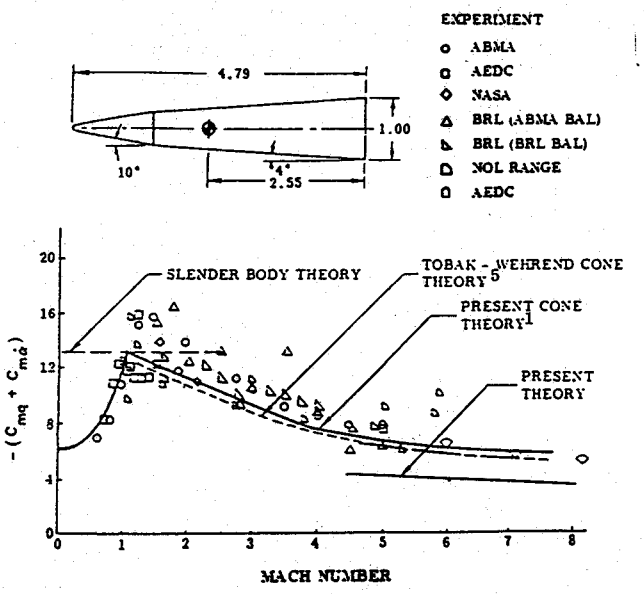

Fig. 9 Comparison between theoretical predictions and experimental results for the pitch damping of a slender biconic configuration.

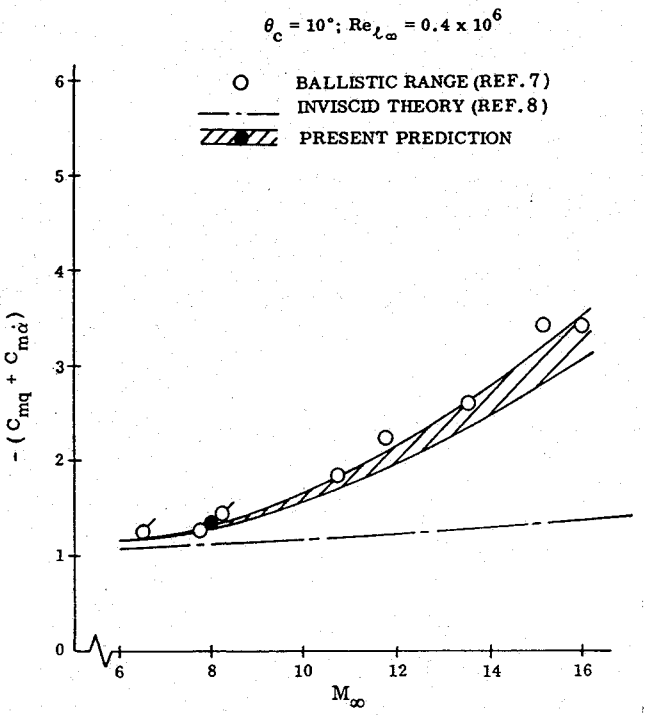

Fig. 10 Comparison between predicted and measured viscous flow effects on the unsteady aerodynamics of a sharp 10-deg cone.[9]

stabilizing component $\Delta^i C_{m\alpha}$ that, when added to the local derivative $C_{m\alpha L}$ (for the chosen geometry), makes the total static stability equal to the Newtonian value (obtained for a slender pointed nose).

Thus, nose bluntness did not degrade the static stability. However, it does degrade the dynamic stability greatly, decreasing the pitch damping, as is shown in the bottom graph. The reason for this effect is explained by the sketch inserted between the static and dynamic stability graphs. The entropy wake existing at the flare at time t, when $\alpha(t)=0$, was generated by the nose at time $t-\Delta t$, when $\alpha(t-\Delta t)>0$. Consequently, the inviscid shear flow is offset from its $\alpha=0$ position at the flare, generating a "residual" force N_F that drives the pitch oscillation. This dynamically destabilizing effect is, of course, dependent on the motion-induced displacement of the wake generator, the blunt nose. It is zero when the nose is stationary and increases with the distance of the oscillation center aft of the nose, as is shown in the bottom graph. Thus, when the center of gravity of the free-flying body is located aft of the midbody, the flare becomes dynamically destabilizing in spite of its full effectiveness in regard to the static stability.

Analysis

For the cylinder-flare geometry in Fig. 3, the inviscid shear flow, the entropy wake in which the aft body is embedded, is defined directly by the nose drag. However, for geometries of current interest, such as blunted slender cones, biconic geometries, and more general axisymmetric shapes, the entropy wake has to be defined by more elaborate means. The existing TRID code[2] is used together with blast-wave theory to define the entropy wake before the embedded Newtonian concept[1,4] is applied.

To define the functions f^* and g^* (Fig. 2) for a general axisymmetric body, the blast wave contribution C_{p0} has to be removed from the surface pressure computed by TRID.[2] After correcting the blast wave pressure C_{p0} for the conical shoulder (Fig. 4), the results shown in Fig. 5 are obtained for the f^* and g^* functions, as determined by the old correlation method[1] and the new TRID-extraction method. A detailed description of the computational procedure is given in the Appendix.

Comparison Between Prediction and Experiment

Figures 6a–6c show the effect of nose bluntness on 5.6-, 7-, and 10-deg cones, respectively. It can be seen that nose bluntness can more than double the Newtonian static stability, while at the same time all but 10–20% of the dynamic stability is lost. Because of the low static margin of the missile RVs the effect of nose bluntness on the static stability varies greatly with x_{CG}, whereas the effect on dynamic stability is relatively insensitive for the range $0.30 \le \Delta\bar{x}/l \le 0.50$ (see Ref. 1). Thus, the low static margin for the 7-deg cone gave a very large effect of nose bluntness on the static stability (Fig. 6b), whereas the effect on dynamic stability was not significantly different from that for 5.6-and 10-deg cones, Figs. 6a and 6c, respectively. By normalizing (dividing) the blunted cone stability derivative by the sharp cone (Newtonian) value, viscous flow effects in the experiment that are the same for the blunted and sharp cones are eliminated, permitting the inviscid prediction to be compared with the viscous experiment. Only for large nose bluntness does one expect any significant differences between the viscous flow effects for blunted and sharp cones. Figures 7a–7c show the highly nonlinear effect of angle of attack on static and dynamic characteristics of 10, 20, and 30% blunt 5.6-deg cones at $M_\infty=14$.

The agreement between prediction and experiment in Figs. 6 and 7 is certainly sufficient for preliminary design purposes. One notes with interest that the agreement between prediction and experiment for the added dynamic prediction capability is as good as that for the already existing static prediction capability through the TRID code.[2]

Figure 8 shows geometries of interest that can be run in the extended embedded Newtonian computer code. Results for one such geometry are shown in Fig. 9. The previous predictions for an equivalent cone (same base area and body length)[5,6] agree better with the experimental results than the present inviscid prediction for the actual geometry. The reason for this is likely to be viscous cross-flow effects, similar to those shown to exist for a pure cone at hypersonic speeds (Fig. 10).[7–9] The reason for the mismatch between earlier inviscid prediction[5] and experiment at low supersonic speeds has also been shown to be viscous flow effects, in this case viscous crossflow effects on boundary-layer transition.[10]

Conclusion

By using previously developed embedded Newtonian flow concepts for unsteady flow, an existing computer program for prediction of the static characteristics of blunted bodies of general shape has been extended to include the unsteady characteristics without any significant increase of the computational time.

Appendix: TRID-Embedded Newtonian Computations

The equations are for a hemisphere-cone forebody geometry (see Fig. 1).

$$C_p = C_\gamma C_{p\text{Newt}} \tag{A1}$$

$$C_\gamma = \begin{cases} 1.01 + 1.31\,[\ell n(10M_\infty \sin\theta_c)]^{-7/3} & M_\infty \sin\theta_c \geq 0.4 \\ 1.625 & M_\infty \sin\theta_c < 0.4 \end{cases} \tag{A2}$$

$$C_{p\max} = \frac{\gamma+3}{\gamma+1}\left[1 - \frac{1.5}{(\gamma+3)M_\infty^2}\right] \tag{A3}$$

$$C_{DN} = \frac{C_{p\max}}{2} \tag{A4}$$

$$C_{p\text{Newt}} = C_{p\max}(\cos\alpha\sin\theta_c + \sin\alpha\cos\theta_c\cos\phi)^2 \tag{A5}$$

$$C_{p\alpha\text{Newt}} = 2C_{p\max}(\cos\alpha\sin\theta_c + \sin\alpha\cos\theta_c\cos\phi) \times (\cos\alpha\cos\theta_c\cos\phi - \sin\alpha\sin\theta_c) \tag{A6}$$

$$C_{pq\text{Newt}} = 2C_{p\max}\frac{x - x_{CG} + r\tan\theta_c}{c}(\cos\alpha\sin\theta_c + \sin\alpha\cos\theta_c\cos\phi)\cos\theta_c\cos\phi \tag{A7}$$

The blast-wave pressure is

$$C_{p0} = \frac{0.081\sqrt{C_{DN}}}{x/d_N} \tag{A8}$$

The asymptotic TRID cone pressure coefficient $C_p(0)$ can be correlated by Eq. (A10) with coefficient C_0 given in Eq. (A9):

$$C_0 = 2.94 + 43.36\,[\ell n(10M_\infty \sin\theta_c)]^{-3} - 0.12M_\infty \sin\theta_c \tag{A9}$$

$$C_p(0) = C_0 C_{p0} + C_{p\text{Newt}} \tag{A10}$$

The f function is then defined as

$$f = \frac{C_p - C_{p0}}{C_p(0)} \tag{A11}$$

$$\Delta z = (x - x_N)\sin\alpha \tag{A12}$$

$$\frac{\partial \Delta z}{\partial \alpha} = (x - x_N)\cos\alpha \tag{A13}$$

$$R^2 = \Delta z^2 + 2r\Delta z\cos\alpha\cos\phi + r^2(\cos^2\alpha\cos^2\phi + \sin^2\phi) \tag{A14}$$

$$\chi = \frac{(r - d_N/2)^2}{d_N x\sqrt{C_{DN}}} \tag{A15}$$

The f function defined in Eq. (A10) can be negative. So we apply the following correction to f so that $f_{b0} \leq f^* \leq 1$; f_0 and f_1 are the values of f at $\chi=0$ and 1, respectively, and f_{b0} is given by the correlation:

$$f_{bo} = 0.165 + \left(\frac{9.65}{M_\infty + 8.7}\right)^3 \tag{A16}$$

$$f^* = f_{bo} + \frac{1 - f_{bo}}{f_1 - f_0}(f - f_0) \tag{A17}$$

$$\frac{\partial f^*}{\partial \Delta z} = 2\chi\left(\frac{df^*}{d\chi}\right)\frac{\Delta z + r\cos\alpha\cos\phi}{r(r - d_N/2)} \tag{A18}$$

$$(C_{p\alpha L})_1 = C_\gamma C_{p\alpha\text{Newt}} f^* \tag{A19}$$

$$(C_{pq})_1 = C_\gamma C_{pq\text{Newt}} f^* \frac{U_\infty}{U} \tag{A20}$$

$$(C_{pq})_2 = 0 \tag{A21}$$

$$(\Delta^i C_{p\alpha})_1 = C_\gamma C_{pq\text{Newt}} \frac{\partial f^*}{\partial \Delta z}\frac{\partial \Delta z}{\partial \alpha} \tag{A22}$$

$$(\Delta^i C_{p\dot{\alpha}})_1 = \left(-\frac{x_{CG} - x_N}{c}\right)\frac{U_\infty}{U}(\Delta^i C_{p\alpha})_1 \tag{A23}$$

$$(\Delta^i C_{p\dot{\alpha}})_2 = 0 \tag{A24}$$

$$C_{p\alpha} = (C_{p\alpha L})_1 + (\Delta^i C_{p\alpha})_1 \tag{A25}$$

$$C_{pq} = (C_{pq})_1 + (C_{pq})_2 + (\Delta^i C_{p\dot{\alpha}})_1 + (\Delta^i C_{p\dot{\alpha}})_2 \tag{A26}$$

The contribution of the nose is

$$(C_{N\alpha})_N = \left(\frac{d_N}{c}\right)^2 (C_{DN})_{\alpha=0} \tag{A27}$$

$$(C_{m\alpha})_N = \left(\frac{d_N}{c}\right)\frac{x_{GC}}{d_N}(C_{N\alpha})_N \tag{A28}$$

$$(C_{mq})_N = -\left(\frac{d_N}{c}\right)^2\left(\frac{x_{CG}}{d_N}\right)^2 (C_{N\alpha})_N \tag{A29}$$

Finally, sum up the contributions from the body and the nose:

$$C_{m\alpha} = -2\int_0^\pi\int_{d_N/2}^r C_{p\alpha}\frac{x - x_{CG} + r\tan\theta_c}{c} \times \cos\theta_c\cos\phi\frac{r\sqrt{1 + \cot^2\theta_c}\,dr\,d\phi}{\pi c^2/4} + (C_{m\alpha})_N \tag{A30}$$

$$C_{mq} = -2\int_0^\pi\int_{d_N/2}^r C_{pq}\frac{x - x_{CG} + r\tan\theta_c}{c} \times \cos\theta_c\cos\phi\frac{r\sqrt{1 + \cot^2\theta_c}\,dr\,d\phi}{\pi c^2/4} + (C_{mq})_N \tag{A31}$$

Acknowledgment

This work was supported by the Lockheed Missiles & Space Company Independent Development Program.

References

[1]Ericsson, L. E., "Unsteady Embedded Newtonian Flow," *Astronautica Acta*, Vol. 18, Nov. 1973, pp. 309–330.

[2]Thomas, P. D., Vinokur, M., Bastianon, R. A., and Conti, R. J., "Numerical Solution for Three-Dimensional Inviscid Supersonic Flow," *AIAA Journal*, Vol. 10, No. 7, 1972, pp. 887–894.

[3]Gravalos, F. G., Edfelt, I. H., and Emmons, H. W., "The Supersonic Flow About a Blunt Body of Revolution for Gases at Chemical Equilibrium," *Proceedings of the IX International Astronautical Congress*,

(Amsterdam, The Netherlands), Aug. 25–30, 1958, pp. 312–332.

[4]Ericsson, L. E., "Generalized Unsteady Embedded Newtonian Flow," *Journal of Spacecraft and Rockets*, Vol. 12, No. 12, 1975, pp. 718–726.

[5]Ericsson, L. E., "Effect of Mach Number on Slender Vehicle Dynamics," *Journal of Spacecraft and Rockets*, Vol. 18, No. 1, 1981, pp. 18–23.

[6]Tobak, M., and Wehrend, W. R., "Stability Derivatives of Cones at Supersonic Speeds," NACA TN 3788, Sept. 1956.

[7]Welsch, C. J., Winchenbach, G. L., and Madigan, A. N., "Free-Flight Investigation of the Aerodynamic Characteristics of a Cone at High Mach Numbers," *AIAA Journal*, Vol. 8, No. 2, 1970, pp. 294–300.

[8]Brong, E. A., "The Unsteady Flow Field about a Right Circular Cone in Unsteady Flight," Air Force Flight Dynamics Laboratory, FDL-TDR-64-148, Wright-Patterson AFB, OH, Jan. 1967.

[9]Ericsson, L. E., "Nonlinear Hypersonic Viscous Crossflow Effects on Slender Vehicle Dynamics," *AIAA Journal*, Vol. 17, No. 6, 1979, pp. 586–593.

[10]Ericsson, L. E., "Viscous Effects on Missile Aerodynamics at Low Angles of Attack," *Journal of Spacecraft and Rockets*, Vol. 18, No. 5, 1981, pp. 401–405.